2-P

NASA TECHNICAL NOTE

NASA TN D-7544

NASA TN D-7544

TRANSONIC FLUTTER STUDY OF A 50.5° CROPPED-DELTA WING WITH TWO REARWARD-MOUNTED NACELLES

by Maynard C. Sandford, Charles L. Ruhlin, and Irving Abel

Langley Research Center
Hampton, Va. 23665

NATIONAL AERONAUTICS AND SPACE ADMINISTRATION • WASHINGTON, D. C. • JUNE 1974

1. Report No.	2. Government Accession No.	3. Recipient's Catalog No.
NASA TN D-7544		

4. Title and Subtitle	5. Report Date
TRANSONIC FLUTTER STUDY OF A 50.5° CROPPED-DELTA WING WITH TWO REARWARD-MOUNTED NACELLES	June 1974
	6. Performing Organization Code
7. Author(s)	8. Performing Organization Report No.
Maynard C. Sandford, Charles L. Ruhlin, and Irving Abel	L-9348
	10. Work Unit No.
9. Performing Organization Name and Address	501-22-04-01
NASA Langley Research Center Hampton, Va. 23665	11. Contract or Grant No.
	13. Type of Report and Period Covered
12. Sponsoring Agency Name and Address	Technical Note
National Aeronautics and Space Administration Washington, D.C. 20546	14. Sponsoring Agency Code

15. Supplementary Notes

Appendix A by Robert N. Desmarais, Langley Research Center.

16. Abstract

Transonic flutter characteristics of three geometrically similar delta-wing models were experimentally determined in the Langley transonic dynamics tunnel at Mach numbers from about 0.6 to 1.2. The models were designed to be simplified versions of an early supersonic transport wing design. The model was an aspect-ratio-1.28 cropped-delta wing with a leading-edge sweep of 50.5°. The flutter characteristics obtained for this wing configuration indicated a minimum flutter-speed index near a Mach number of 0.92 and a transonic compressibility dip amounting to about a 27-percent decrease in the flutter-speed index relative to the value at a Mach number of 0.6. Analytical studies were performed for one wing model at Mach numbers of 0.6, 0.7, 0.8, and 0.9 by using both doublet-lattice and lifting-surface (kernel-function) unsteady aerodynamic theory. A comparison of the analytical and experimental flutter results showed good agreement at all Mach numbers investigated.

17. Key Words (Suggested by Author(s))	18. Distribution Statement
Transonic flutter Cropped-delta wing Aeroelasticity Structural dynamics	Unclassified – Unlimited STAR Category 32

19. Security Classif. (of this report)	20. Security Classif. (of this page)	21. No. of Pages	22. Price*
Unclassified	Unclassified	29	$3.25

*For sale by the National Technical Information Service, Springfield, Virginia 22151

TRANSONIC FLUTTER STUDY OF A 50.5° CROPPED-DELTA WING WITH TWO REARWARD-MOUNTED NACELLES

By Maynard C. Sandford, Charles L. Ruhlin,
and Irving Abel
Langley Research Center

SUMMARY

Transonic flutter characteristics of three geometrically similar delta-wing models were experimentally determined in the Langley transonic dynamics tunnel at Mach numbers from about 0.6 to 1.2. The models were designed to be simplified versions of an early supersonic transport wing design. The model was an aspect-ratio-1.28 cropped-delta wing with a leading-edge sweep of 50.5°. The flutter characteristics obtained for this wing configuration indicated a minimum flutter-speed index near a Mach number of 0.92 and a transonic compressibility dip amounting to about a 27-percent decrease in the flutter-speed index relative to the value at a Mach number of 0.6. Analytical studies were performed for one wing model at Mach numbers of 0.6, 0.7, 0.8, and 0.9 by using both doublet-lattice and lifting-surface (kernel-function) unsteady aerodynamic theory. A comparison of the analytical and experimental flutter results showed good agreement at all Mach numbers investigated.

INTRODUCTION

Although aircraft have been designed for a number of years to operate at supersonic speeds, there is still considerable need for a better understanding of transonic flutter characteristics, since traversal of this range is necessary to reach supersonic flight. Past experience has shown that the transonic Mach number range is the most critical since the minimum flutter dynamic pressure usually occurs there. Since transonic unsteady aerodynamic theory is not developed to the stage that it can be used with confidence for flutter prediction, it is necessary to rely upon experimental studies to provide transonic flutter data. A review of the recent literature indicates a noticeable lack of transonic flutter studies of a research nature for configurations of current interest.

The purpose of this paper is to present the results of a transonic flutter investigation of three geometrically similar cropped-delta wing models that were studied to establish baseline data for the design of a model for use in active flutter-suppression studies. The models were designed to be simplified versions of an early supersonic transport wing. The model was an aspect-ratio-1.28 cropped-delta wing with a leading-edge sweep

of 50.5° and a taper ratio of 0.127. Two high-fineness-ratio bodies simulating mass and inertia characteristics of the engine nacelles were mounted on the underside of the models. The differences between the models were size, mass, and stiffness level and distribution. Based on the full-scale design, there were two 1/36-size models and one 1/17-size model. Flutter boundaries were experimentally determined in the Langley transonic dynamics tunnel over the Mach number range from about 0.60 to 1.20. Analytical flutter results were obtained for the 1/17-size model at Mach numbers of 0.6, 0.7, 0.8, and 0.9. The experimental and analytical results are presented and discussed in the main body of the paper. Some of the details of the analysis and a discussion of the method used to display graphically the measured modal data which were determined for use in the flutter calculations are presented in appendixes A and B.

SYMBOLS

b	one-half mean geometric chord of wing, 0.281 m for 1/36-size model and 0.596 m for 1/17-size model
c	streamwise chord, m
f	flutter frequency, Hz
f_i	natural frequency of ith structural vibration mode (i = 1, 2, . . ., N), Hz
I_N	engine nacelle pitch moment of inertia about center of gravity, kg-m^2
M	Mach number
m_N	mass of nacelle, kg
m_W	mass of semispan wing panel (without nacelles), kg
m_{WN}	total mass of wing configuration, includes semispan wing and nacelles, kg
t	airfoil thickness, m
V	free-stream velocity, m/s

v volume of a conical frustum having wing chord at root (BL 0) as base diameter, wing tip chord as upper diameter, and wing semispan as height, 0.1246 m^3 for 1/36-size model and 1.183 m^3 for 1/17-size model

X streamwise coordinate, origin at FS 0 (see fig. 2), m

x/c fraction of local streamwise chord

Y spanwise coordinate, origin at BL 0 (see fig. 2), m

Z_i nondimensional vertical displacement of ith structural mode, normalized to FS 50 (see table II(a))

η nondimensional spanwise coordinate

μ mass-density ratio, $\dfrac{m_{WN}}{\text{Test medium density} \times v}$

Abbreviations:

BL buttock line (see fig. 2), m

FS fuselage station (see fig. 2), m

DESCRIPTION OF MODELS

General

Three semispan delta-wing models were used in the present investigation. The models had similar planforms but differed in size, mass, and stiffness properties. The models were simplified representations of an early supersonic transport wing design. Photographs and sketches of the models are presented in figures 1 and 2. There were two 1/36-size models, referred to hereafter as wing A and wing B, and there was a 1/17-size model, referred to hereafter as wing C. Relative to the full-scale design, wing A was stiffer than wing B, and wing C was the least stiff of the three models.

The model was an aspect-ratio-1.28 cropped-delta wing with a leading-edge sweepback angle of 50.5° and a taper ratio of 0.127. The symmetrical circular-arc airfoil section had a thickness-to-chord ratio of 0.03. Two high-fineness-ratio bodies simulating the mass and inertia characteristics of engine nacelles were mounted on the underside of

the wing at about 22 and 44 percent of the wing semispan. Each nacelle provided a concentrated mass of about one-half of the wing-panel mass.

The model was cantilever-mounted from the tunnel side wall. (See fig. 1.) The model was clamped to a relatively rigid mounting block which was attached to a turntable in the tunnel wall. A simulated fuselage shape which extended ahead of and behind the wing was attached to the mounting block. This mounting arrangement brought the wing root outside the tunnel wall boundary layer. A photograph of a typical model installed in the tunnel is shown in figure 1 with the lower fuselage fairing removed.

Construction

Each of the three semispan wing models was constructed of an aluminum-alloy plate and covered with balsa wood which was contoured to the proper airfoil shape. Some details of model construction are illustrated in figure 3. The plate thickness was tapered linearly in the spanwise direction in two sections. The break in the taper was at the 0.53 nondimensional semispan station. The plate thickness at the break, root, and tip stations is presented in the table in figure 3 for all three models. Holes were chemically milled through the aluminum plate in order to simulate a rib and spar pattern. The balsa-wood covering was fabricated by gluing strips of balsa wood (with the grain oriented chordwise) to the top and bottom of the aluminum-alloy plate to form a continuous covering. The balsa-wood covering was then cut and sanded to produce the proper airfoil shape and planform dimensions since the balsa wood overhung the aluminum plate. Two identical engine nacelles were constructed for each of the three models tested. Each nacelle consisted of a cylindrical centerbody with an ogive nose and a conical tail fairing. The centerbody was a thick-wall steel tube and was ballasted with lead weights. The nose and tail fairing were constructed of balsa wood. Electrical resistance wire strain gages were mounted on the main structural plate of each wing model near the root to indicate deflections in bending and torsion.

Physical Properties

Stiffness.- The primary stiffness properties of each model were obtained from the aluminum-alloy plate. Since the spar and rib pattern was identical for all models, stiffness variations between models were accomplished by varying the plate thickness. (See table in fig. 3.) Wing A and wing B differed both in stiffness level and stiffness distribution, wing A having the higher stiffness level. Wing C was built to have the same stiffness distribution as wing A but the scaled stiffness level was reduced for the convenience of obtaining flutter at low dynamic pressures.

Mass.- Some measured total mass and inertia properties of the three wing panels and the engine nacelles are presented in table I. Additional mass data were obtained for

wing C in the form of generalized masses and are presented in table II(b). The mass distribution of wing C was designed to be the same as that of wing A but the mass distribution differed between wing A and wing B. Generalized masses were determined by using the method of displaced frequencies described in references 1 and 2.

Frequencies.- The nodal patterns and corresponding frequencies for the first six natural modes for wing A and wing B cantilever-mounted in the wind tunnel are presented in figure 4. A comparison of the nodal patterns shows that the three lowest modes are very similar.

A more detailed determination of the vibration characteristics of wing C was made for use in analytical studies. In addition to obtaining natural frequencies and nodal patterns as was done for wing A and wing B, the actual mode shapes and corresponding generalized masses were experimentally determined for wing C. (See table II.) The mode shapes were measured at 54 stations on the wing surface (six spanwise stations and nine chordwise stations). Six additional points were added to define the engine motion. Each station number, coordinate location, and the nondimensional vertical displacement for the first nine natural modes are presented in table II(a). Computer graphic display of the mode shapes for the first nine natural modes of wing C are shown in figure 5. A discussion of the methods used to generate these computer plots of the mode shapes is described in appendix A.

WIND-TUNNEL AND TEST PROCEDURES

Wind Tunnel

This investigation was conducted in the Langley transonic dynamics tunnel which has a 16-foot-square test section with cropped corners and is a return-flow, variable-pressure, slotted-throat wind tunnel. It is capable of operation at stagnation pressures from near vacuum to slightly above atmospheric and at Mach numbers from 0 to 1.2. Mach number and dynamic pressure can be varied independently with either air or Freon used as a test medium. For the present investigation, only Freon was used. The tunnel is equipped with four quick-opening bypass valves which can be operated when flutter occurs in order to reduce rapidly the dynamic pressure and Mach number in the test section. A more complete description of the wind tunnel is given in reference 3.

Test Procedure

The usual test procedure was to set a given stagnation pressure in the tunnel and vary the Mach number (and dynamic pressure) from a low subsonic value up to conditions where the model fluttered or the maximum Mach number obtainable at this pressure was reached. At flutter, the bypass valves were opened to reduce quickly the dynamic pressure and Mach number. Similar Mach number sweeps at various stagnation pressures

were made to define the flutter boundaries up to the transonic dip (Mach number 0.92). For some flutter points, a constant Mach number was maintained while the stagnation pressure was increased until flutter occurred. Throughout these tests the model angle of attack was adjusted to minimize static loads on the wing.

During the tests, strain-gage signals from the model were monitored continuously and recorded on direct readout recorders. Visual records of the models were provided by high-speed motion pictures taken from the side and from the rear of the model. Also, a closed-circuit television tape system was used to provide a quick review of the flutter occurrences. Tunnel conditions were automatically recorded.

RESULTS AND DISCUSSION

General

From visual observations and high-speed motion pictures, the flutter modes for all three wing models resembled closely the second natural vibration mode with some coupling of the fundamental bending mode. Therefore, the second-mode frequency was used to normalize the test results. A flutter analysis was performed on the largest size model, wing C, by using measured mode shapes, generalized masses, and natural frequencies of the first nine modes. Analytical flutter results were obtained for comparison with the wing C model at Mach numbers of 0.6, 0.7, 0.8, and 0.9.

The experimental flutter results for wing A, wing B, and wing C are compiled in table III and presented in figures 6, 7, and 8. The analytical flutter results for wing C are presented in figure 9.

Experimental Results

The experimental flutter results for wing A, wing B, and wing C are presented in figure 6 in terms of dynamic-pressure variations with Mach number. For the purpose of correlating the flutter results of the three wing models, these flutter data are presented in figure 7 in terms of the variation of the flutter-speed index with Mach number. This parameter is designed to account for the effects on flutter of varying model geometric size, relative stiffness, and mass levels for models of similar planform and similar stiffness and mass distributions, provided that the flutter mode does not change and that any significant mass-ratio effects are similar. Also included in figure 7 are variations in mass ratio and flutter-frequency ratio with Mach number. Comparisons of the mass-ratio and frequency-ratio results indicate good agreement for all three models throughout the Mach number range covered and also indicate that mass-ratio effects were not significant and that the flutter modes of all three wings are the same. The flutter-speed-index parameters show good correlation for wings A and C which had similar mass and stiffness

distributions. Since these two models were designed to be different in geometric size and in relative stiffness level, it is evident from these data that for these differences the flutter-speed index is an adequate normalizing parameter. However, a large difference exists in the flutter-speed-index values for wing A and wing B (same geometric size models). This difference is not surprising since these two models were designed to have different mass and stiffness distributions. Note that this large difference in flutter-speed index is nearly constant over the Mach number range. Therefore, the flutter-speed-index boundaries shown in figure 7 were normalized by their corresponding value at about $M = 0.6$ and presented in figure 8. A single curve drawn through the data points as shown in figure 8 indicates that the compressibility effects for all three wings were similar. The flutter boundary shown in figure 8 indicates a minimum flutter-speed index near a Mach number of 0.92 and a transonic compressibility dip amounting to about a 27-percent decrease in the flutter-speed index relative to the value at a Mach number of 0.6.

Analytical Results

A comparison of calculated and experimental flutter results for wing C is presented in figure 9. The data are presented as a variation of the flutter-speed-index parameter, flutter frequency, and mass-density ratio with Mach number. The calculated results correspond to a matched point with respect to the flow velocity at the experimental flutter point for that Mach number. (The matched point is determined by plotting the calculated flutter speed as a function of flow density from which the density corresponding to the tunnel flow velocity at each Mach number is determined.) Throughout the Mach number range the calculated flutter-speed index, flutter frequency, and mass-density ratio agree closely both in trend and level with the experimental results. During the analysis it was found that the first six measured modes were required to achieve the results presented. Additional modes up to nine did not change the analytical flutter results from those obtained by using the first six modes. A brief discussion of the doublet-lattice and kernel-function calculations used in these analytical studies are given in appendix B.

CONCLUDING REMARKS

An experimental flutter study was made in the Langley transonic dynamics tunnel at Mach numbers from 0.6 to 1.2 for three wing models which had the same planform but which differed in size, stiffness, and mass properties. The model was an aspect-ratio-1.28 cropped-delta wing with a leading-edge sweep of 50.5° and a taper ratio of 0.127. Two high-fineness-ratio bodies simulating engine nacelles were mounted on the underside of the wing surface. Analytical flutter studies were performed on the largest model by using nine experimentally measured structural mode shapes, generalized masses, and natural frequencies. Some concluding remarks about the present flutter study are

1. All three wing models investigated showed a minimum flutter-speed index near a Mach number of 0.92 and a transonic compressibility dip amounting to about a 27-percent decrease in the flutter-speed index relative to the value at a Mach number of 0.6.

2. Analytical flutter studies using kernel-function and doublet-lattice aerodynamics showed good agreement with experimental flutter results at Mach numbers of 0.6, 0.7, 0.8, and 0.9.

Langley Research Center,
National Aeronautics and Space Administration,
Hampton, Va., February 19, 1974.

APPENDIX A

COMPUTER-GENERATED PLOTS OF THE MODE SHAPES

By Robert N. Desmarais
Langley Research Center

The plots of the measured mode shapes appearing as figures 5(a) and 5(b) were prepared by use of the graphics subroutines of a program that is used to compute slopes and deflections for subsequent aerodynamic force calculations. The program interpolates the measured mode shapes by using a surface spline described in reference 4. That is, each mode is represented by an interpolation function W given by

$$W(X,Y) = a_1 + a_2X + a_3Y + \sum_{i=1}^{N} b_i r_i^2 \log_e r_i^2 \tag{A1}$$

where

$$r_i^2 = (X - X_i)^2 + (Y - Y_i)^2$$

The coefficients a_i and b_i are obtained by solving the system of $N + 3$ equations

$$Z_j = a_1 + a_2X_j + a_3Y_j + \sum_{i=1}^{N} b_i r_{ij}^2 \log_e r_{ij}^2 \qquad (i,j = 1 \ldots N) \tag{A2}$$

where

$$r_{ij}^2 = (X_j - X_i)^2 + (Y_j - Y_i)^2$$

and

$$\sum_{i=1}^{N} b_i = \sum_{i=1}^{N} b_i X_i = \sum_{i=1}^{N} b_i Y_i = 0 \tag{A3}$$

The set of N points used to construct equations (A2) and (A3) was obtained by combining the N_m measured data points listed in table II with nine additional equispaced points along the root chord with zero deflections. An additional N_m points were generated as mirror images of the measured data points because it was assumed that the mode shapes were symmetrical. Thus, a total of $2N_m + 9$ points were used to construct $W(X,Y)$

where $N_m = 54$ for modes 1 and 2 and $N_m = 60$ for modes 3 to 9. The mirror image points insure that $W(X,Y)$ is an even function of Y and the nine points along the root insure that $W(X,0) = 0$. Thus, $W(X,Y)$ closely approximates the geometric boundary conditions of a cantilevered plate.

The oblique projection plots were constructed by using the interpolation function $W(X,Y)$ described to compute the deflections over a program-generated rectangular grid and then connecting the oblique projections of the grid points with straight lines. Each grid rectangle has a chordwise length equal to 1/20th of the root chord and has approximately the same spanwise width. (The actual width was adjusted so that the tip would lie on a grid boundary.) For this projection, the X-axis is rotated 32° forward of the plane of the paper and the X,Y plane is 30° below the horizontal.

The contour plots were drawn by using a program-generated equilateral triangular grid. Within each grid triangle, each contour line segment is determined by the intersection of two planes. One is the tilted plane determined by the elevation of the three grid vertices and the other is the horizontal plane of the contour level. The elevation of the vertices of each triangle is computed from equation (A1).

APPENDIX B

FLUTTER CALCULATIONS

General

Flutter calculations were performed for the wing C model at Mach numbers of 0.6, 0.7, 0.8, and 0.9. The generalized aerodynamic forces were formulated through the use of doublet-lattice aerodynamics at all Mach numbers and kernel-function aerodynamics at $M = 0.6$ and $M = 0.9$. Two different aerodynamic theories were used for comparison purposes. All flutter calculations were made by use of the nine experimentally measured structural modes, generalized masses, and natural frequencies presented in figure 5 and table II. The effect of varying flow density on the calculated flutter speed was determined so that a matched point, corresponding to the tunnel flow velocity, was determined at each Mach number.

Doublet-Lattice Calculations

The doublet-lattice flutter calculations were based on the method described in reference 5. In order to calculate the pressure distribution on an oscillating wing, the method of reference 5 subdivides the lifting surface into an array of trapezoidal boxes arranged in strips parallel to the airstream. The lifting surface is then replaced with an unsteady vortex lattice composed of doublets located along the quarter-chord of each box. The downwash boundary condition is then satisfied at the three-quarter chord of each box. The model was divided into 160 boxes. The boxes are arranged in 16 streamwise strips with 10 boxes per strip. Figure 10 shows the paneling scheme and gives the location of the box edges in terms of the wing span η and the local streamwise chord x/c. The downwash boundary condition on the wing is then evaluated by equating the downwash to the slope and deflection measured for each structural mode. Since the grid used to measure the structural modes (fig. 11) is not the same as the required aerodynamic grid (fig. 10), natural cubic spline functions similar to those described in reference 6 were used to determine the required slopes and deflections. The aerodynamics are then combined with the mass and stiffness representation of the model in a conventional flutter analysis to yield the required flutter speed.

Kernel-Function Calculations

All kernel-function calculations were obtained by a method similar to that described in reference 7. In this method the pressure distribution on an oscillating wing is calculated by numerically solving a linear integral equation which relates the pressure distribution to the downwash specified at known control points. The downwash is related in

turn to the mode shape for each structural mode. Thirty-six control points are used in these calculations. The points are located at η = 0.121, 0.355, 0.568, 0.748, 0.885, and 0.971 along the wing semispan and at x/c = 0.057, 0.216, 0.440, 0.677, 0.874, and 0.985 along the local streamwise chord. The locations of these control points are shown by circles in figure 10. Once again, spline interpolation functions were used extensively to determine the slopes and deflections for each structural mode at the control points. The kernel-function aerodynamics are then combined with the mass and stiffness representation of the model to yield the required flutter speed.

REFERENCES

1. Gauzy, H.: Measurement of Inertia and Structural Damping. AGARD Manual on Aeroelasticity, Part IV, Chapter 3, Oct. 1968.

2. Abel, Irving: A Wind-Tunnel Evaluation of Analytical Techniques for Predicting Static Stability and Control Characteristics of Flexible Aircraft. NASA TN D-6656, 1972.

3. Ruhlin, Charles L.; Sandford, Maynard C.; and Yates, E. Carson, Jr.: Wind-Tunnel Flutter Studies of the Sweptback T-Tail of a Large Multijet Cargo Airplane at Mach Numbers to 0.90. NASA TN D-2179, 1964.

4. Harder, Robert L.; and Desmarais, Robert N.: Interpolation Using Surface Splines. J. Aircraft, vol. 9, no. 2, Feb. 1972, pp. 189-191.

5. Albano, Edward; and Rodden, William P.: A Doublet-Lattice Method for Calculating Lift Distributions on Oscillating Surfaces in Subsonic Flows. AIAA J., vol. 7, no. 2, Feb. 1969, pp. 279-285.

6. Greville, T. N. E.: Spline Functions, Interpolation, and Numerical Quadrature. Mathematical Methods for Digital Computers, Vol. II. Anthony Ralston and Herbert S., Wilf, eds., John Wiley & Sons, Inc., c.1967, pp. 156-168.

7. Watkins, Charles E.; Woolston, Donald S.; and Cunningham, Herbert J.: A Systematic Kernel Function Procedure for Determining Aerodynamic Forces on Oscillating or Steady Finite Wings at Subsonic Speeds. NASA TR R-48, 1959.

TABLE I.- MEASURED MASS PROPERTIES

Model	Mass, kg (a)	Center of gravity		Inertia about center of gravity			$\frac{m_N}{m_W}$	$\frac{I_N}{m_N b^2}$
		BL, m	FS, m	Pitch, $kg\text{-}m^2$	Yaw, $kg\text{-}m^2$	Roll, $kg\text{-}m^2$		
Wing A:								
Wing	2.027	0.132	0.471	0.0853	0.0903	0.0417	—	—
Inboard nacelle	1.039	.137	.752	.0056	.0056	—	0.513	0.068
Outboard nacelle	1.033	.268	.752	.0054	.0054	—	.509	.067
Total - wing and nacelles	4.099	.168	.614	.1756	.1948	.0556	—	—
Wing B:								
Wing	1.329	0.167	0.505	0.0494	0.0676	0.0275	—	—
Inboard nacelle	.661	.137	.752	.0037	.0037	—	0.496	0.072
Outboard nacelle	.658	.268	.752	.0037	.0037	—	.494	.072
Total - wing and nacelles	2.649	.185	.628	.0969	.1103	.0340	—	—
Wing C:								
Wing	14.215	—	—	—	—	—	—	—
Inboard nacelle	6.480	0.291	1.617	0.1470	0.1470	—	0.456	0.064
Outboard nacelle	6.480	.568	1.617	0.1470	.1470	—	.456	.064
Total - wing and nacelles	27.175	—	—	—	—	—	—	—

(a) All wing mass properties are for semispan wing outboard of BL 0.0.

TABLE II.- TABULATED MEASURED MODE SHAPE AND GENERALIZED MASS DATA FOR WING C MODEL

[X and Y are in meters. Z_1 to Z_9 are normalized to station 50.]

(a) Mode shape

STA	X	Y	Z_1	Z_2	Z_3	Z_4	Z_5	Z_6	Z_7	Z_8	Z_9
1	.264	.153	.009	.007	-.001	-.003	.010	-.016	.022	.034	.041
2	.438	.153	.008	.009	-.009	-.007	.009	-.025	.031	.049	.063
3	.611	.153	.012	.010	-.015	-.011	.018	-.023	.036	.057	.071
4	.785	.153	.016	.009	-.024	-.015	.033	-.014	.040	.061	.066
5	.974	.153	.021	.005	-.027	-.013	.063	.010	.033	.048	.036
6	1.164	.153	.027	-.001	-.034	-.011	.103	.038	.030	.034	-.003
7	1.337	.153	.035	-.009	-.046	-.004	.143	.058	.028	.025	-.047
8	1.511	.153	.036	-.026	-.070	.027	.154	.050	.024	.018	-.082
9	1.684	.153	.051	-.053	-.116	.082	.124	.014	.021	.009	-.083
10	.607	.450	.038	.044	-.151	-.095	-.022	-.228	.193	.323	.384
11	.740	.450	.053	.046	-.176	-.106	-.011	-.207	.194	.319	.351
12	.874	.450	.070	.041	-.187	-.112	.014	-.150	.173	.280	.284
13	1.008	.450	.090	.033	-.189	-.110	.043	-.063	.141	.216	.199
14	1.154	.450	.112	.017	-.159	-.099	.083	.048	.100	.134	.097
15	1.300	.450	.137	-.004	-.168	-.085	.119	.161	.060	.056	-.002
16	1.434	.450	.164	-.041	-.144	-.053	.135	.234	.039	.008	-.087
17	1.568	.450	.186	-.094	-.091	-.006	.105	.208	.039	.006	-.138
18	1.702	.450	.234	-.160	-.012	.049	.055	.118	.056	.040	-.193
19	.918	.721	.174	.130	-.425	-.246	-.229	-.608	.265	.466	.290
20	1.016	.721	.209	.125	-.406	-.237	-.221	-.530	.194	.362	.186
21	1.114	.721	.235	.114	-.352	-.210	-.189	-.389	.115	.243	.107
22	1.212	.721	.264	.103	-.301	-.187	-.159	-.257	.041	.124	.050
23	1.319	.721	.296	.085	-.225	-.157	-.114	-.101	-.039	-.011	.037
24	1.425	.721	.337	.060	-.135	-.125	-.072	.040	-.110	-.135	.076
25	1.523	.721	.378	.032	-.039	-.095	-.044	.142	-.169	-.233	.126
26	1.621	.721	.412	0.000	.066	-.066	-.016	.229	-.228	-.326	.194
27	1.719	.721	.449	-.036	.180	-.036	.010	.304	-.284	-.409	.272
28	1.182	.950	.428	.305	-.365	-.197	-.572	-1.167	-.024	.263	-.601
29	1.250	.950	.436	.304	-.277	-.150	-.500	-.971	-.072	.157	-.575
30	1.317	.950	.478	.307	-.191	-.100	-.434	-.805	-.123	.050	-.531
31	1.384	.950	.514	.312	-.095	-.043	-.339	-.603	-.166	-.056	-.460
32	1.457	.950	.547	.319	.018	.025	-.231	-.372	-.212	-.174	-.355
33	1.531	.950	.580	.326	.131	.091	-.126	-.127	-.255	-.294	-.232
34	1.598	.950	.605	.329	.229	.152	-.026	.090	-.295	-.400	-.117
35	1.665	.950	.642	.345	.346	.228	.099	.337	-.304	-.482	.048
36	1.733	.950	.688	.352	.463	.294	.209	.594	-.352	-.612	.185
37	1.383	1.124	.687	.606	.102	.203	-.320	-.945	.021	.237	-.950
38	1.427	1.124	.717	.619	.207	.269	-.178	-.694	.057	.224	-.751
39	1.471	1.124	.734	.642	.307	.342	-.048	-.438	.096	.211	-.559
40	1.515	1.124	.758	.670	.409	.432	.092	-.189	.130	.195	-.354
41	1.563	1.124	.791	.686	.518	.509	.242	.092	.168	.187	-.116
42	1.611	1.124	.815	.707	.619	.585	.384	.363	.209	.158	.112
43	1.655	1.124	.839	.722	.710	.647	.519	.620	.233	.125	.325
44	1.699	1.124	.863	.724	.798	.712	.646	.866	.265	.097	.538
45	1.743	1.124	.893	.748	.886	.774	.792	1.127	.303	.072	.761
46	1.508	1.233	.921	.915	.674	.748	.487	.066	.696	.868	.037
47	1.537	1.233	.920	.937	.747	.803	.598	.291	.767	.897	.246
48	1.567	1.233	.946	.951	.829	.879	.734	.520	.839	.927	.505
49	1.596	1.233	.972	.974	.907	.925	.859	.737	.905	.961	.754
50	1.629	1.233	1.000	1.000	1.000	1.000	1.000	1.000	1.000	1.000	1.000
51	1.661	1.233	.994	1.009	1.074	1.067	1.144	1.268	1.051	1.033	1.272
52	1.690	1.233	1.017	1.034	1.178	1.122	1.290	1.511	1.143	1.066	1.505
53	1.720	1.233	1.019	1.035	1.235	1.155	1.410	1.720	1.196	1.075	1.766
54	1.750	1.233	1.051	1.040	1.294	1.220	1.531	1.950	1.251	1.096	1.975
55	1.709	.567	*	*	.242	-.041	-.006	-.073	.036	.056	.018
56	1.591	.567	*	*	.035	-.068	.043	.147	-.009	-.040	.030
57	1.473	.567	*	*	.113	-.095	.065	.240	-.023	-.069	.035
58	1.692	.291	*	*	.261	.211	-.077	-.032	.003	.017	.015
59	1.537	.291	*	*	.151	.056	.115	.120	.034	.026	-.118
60	1.382	.291	*	*	.105	-.018	.162	.144	.044	.037	-.092

* DEFLECTIONS AT STATIONS 55 THROUGH 60 WERE NOT MEASURED FOR MODES 1 AND 2.

TABLE II.- TABULATED MEASURED MODE SHAPE AND GENERALIZED MASS DATA FOR WING C MODEL – Concluded

(b) Generalized mass

Mode	Natural frequency, hertz	Generalized mass, grams
1	7.8	1536
2	16.4	489
3	24.1	1065
4	25.4	720
5	38.2	1885
6	43.3	820
7	45.9	351
8	48.2	2520
9	58.1	1445

TABLE III.- COMPILATION OF EXPERIMENTAL RESULTS

[All data obtained in Freon medium]

Model configuration	Mach number	Dynamic pressure, kN/m^2	Velocity, m/s	Test medium density, kg/m^3	Reynolds number (a)	f, Hz	f/f_2	μ	$\frac{V}{b(2\pi f_2)\sqrt{\mu}}$	$\frac{\frac{V}{b(2\pi f_2)\sqrt{\mu}}}{\left(\frac{V}{b(2\pi f_2)\sqrt{\mu}}\right)_{M\approx 0.6}}$
Wing A	0.665	13.15	103.14	2.472	11.04×10^6	28.2	0.814	13.31	0.462	1.000
	.873	9.00	134.72	.992	5.85	26.3	.759	33.18	.382	.827
	.893	7.78	136.64	.834	5.06	25.2	.727	39.43	.355	.770
	.920	6.87	140.91	.692	4.32	23.8	.687	47.57	.333	.722
	.929	7.77	145.33	.736	4.60	24.0	.693	44.68	.355	.769
	1.000	11.00	155.54	.909	6.11	26.6	.768	36.19	.422	.914
Wing B	0.620	9.77	94.79	2.175	9.14×10^6	26.2	0.887	9.78	0.580	1.000
	.777	8.41	118.57	1.197	6.32	24.7	.836	17.76	.538	.928
	.924	5.61	142.46	.553	3.45	20.9	.707	38.45	.440	.758
	1.191	8.80	182.76	.527	4.25	22.7	.768	40.37	.550	.949
Wing C	0.603	8.68	93.52	1.985	17.01×10^6	12.9	0.791	11.60	0.450	1.000
	.708	7.97	109.74	1.324	13.36	12.5	.766	17.38	.431	.958
	.811	7.21	124.85	.925	10.76	12.1	.741	24.88	.410	.912
	.907	5.55	145.32	.526	6.69	11.0	.674	43.78	.358	.796

(a) Reynolds number based on mean geometric chord of wing.

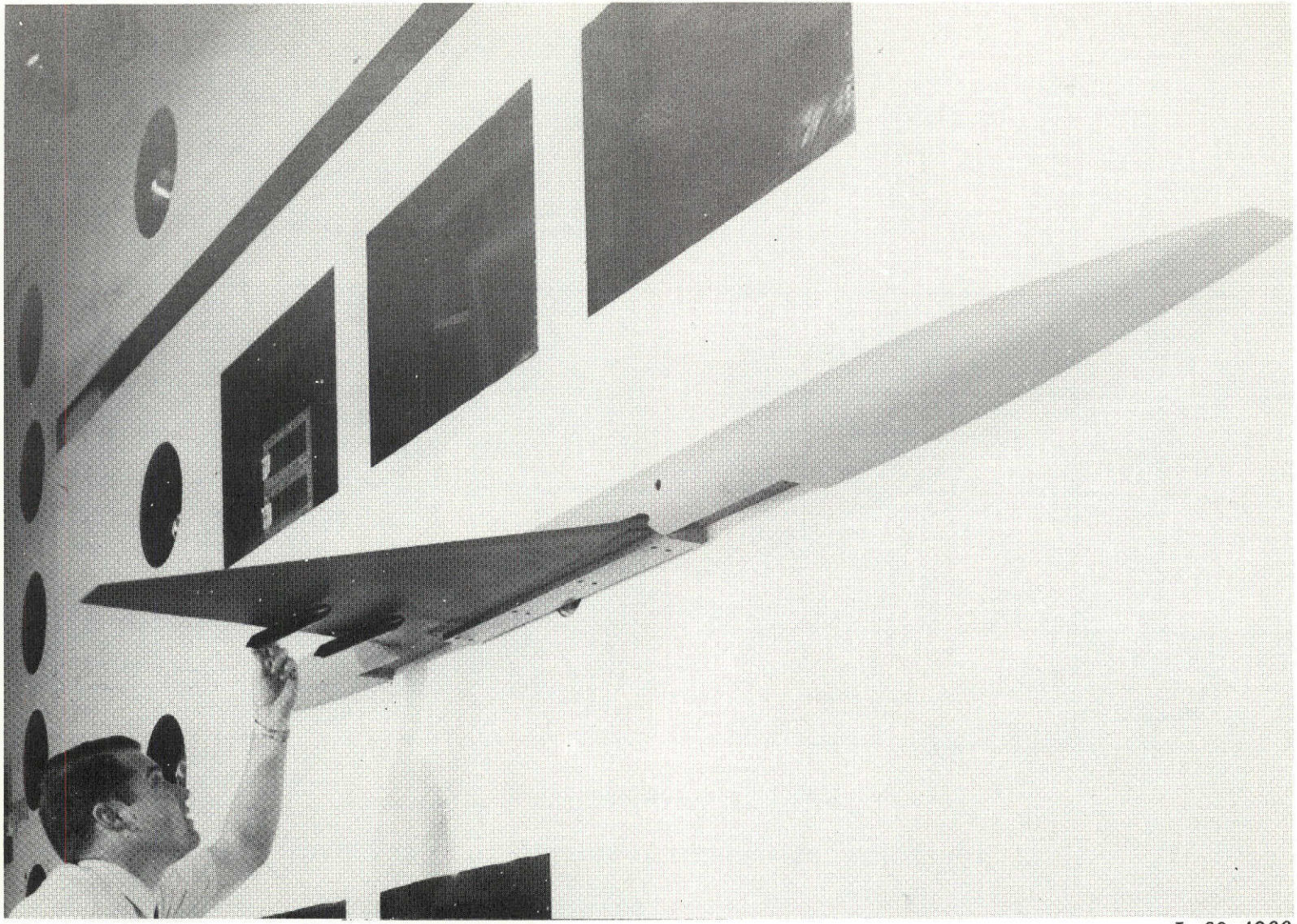

L-69-4866

Figure 1.- A 1/36-size model mounted in the Langley transonic dynamics tunnel.

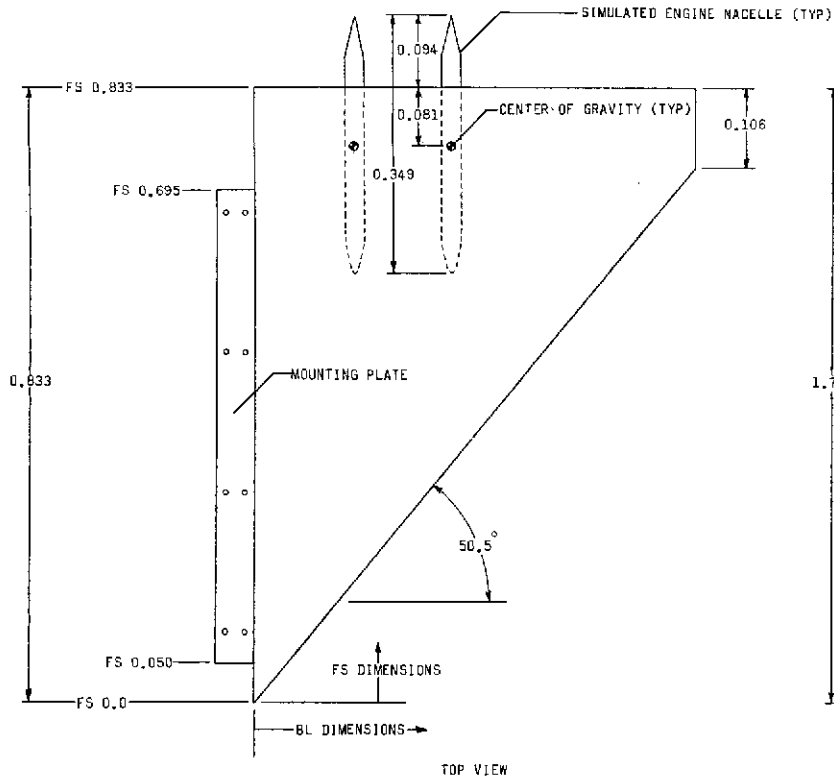

(a) 1/36-size model.

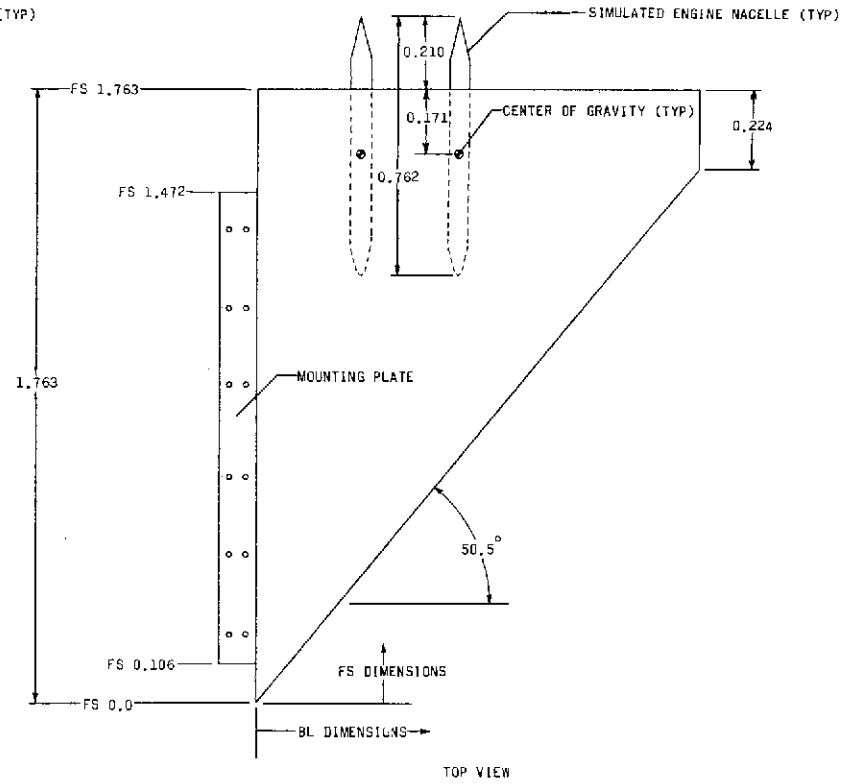

(b) 1/17-size model.

Figure 2.- Sketches of models. All dimensions are in meters.

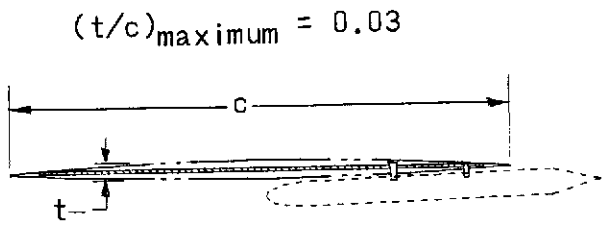

Wing	Internal plate thickness, m		
	η = 0.0	η = .53	η = 1.0
A	0.009525	0.003810	0.000457
B	.005004	.002692	.000635
C	.016408	.006502	.000711

Section A-A

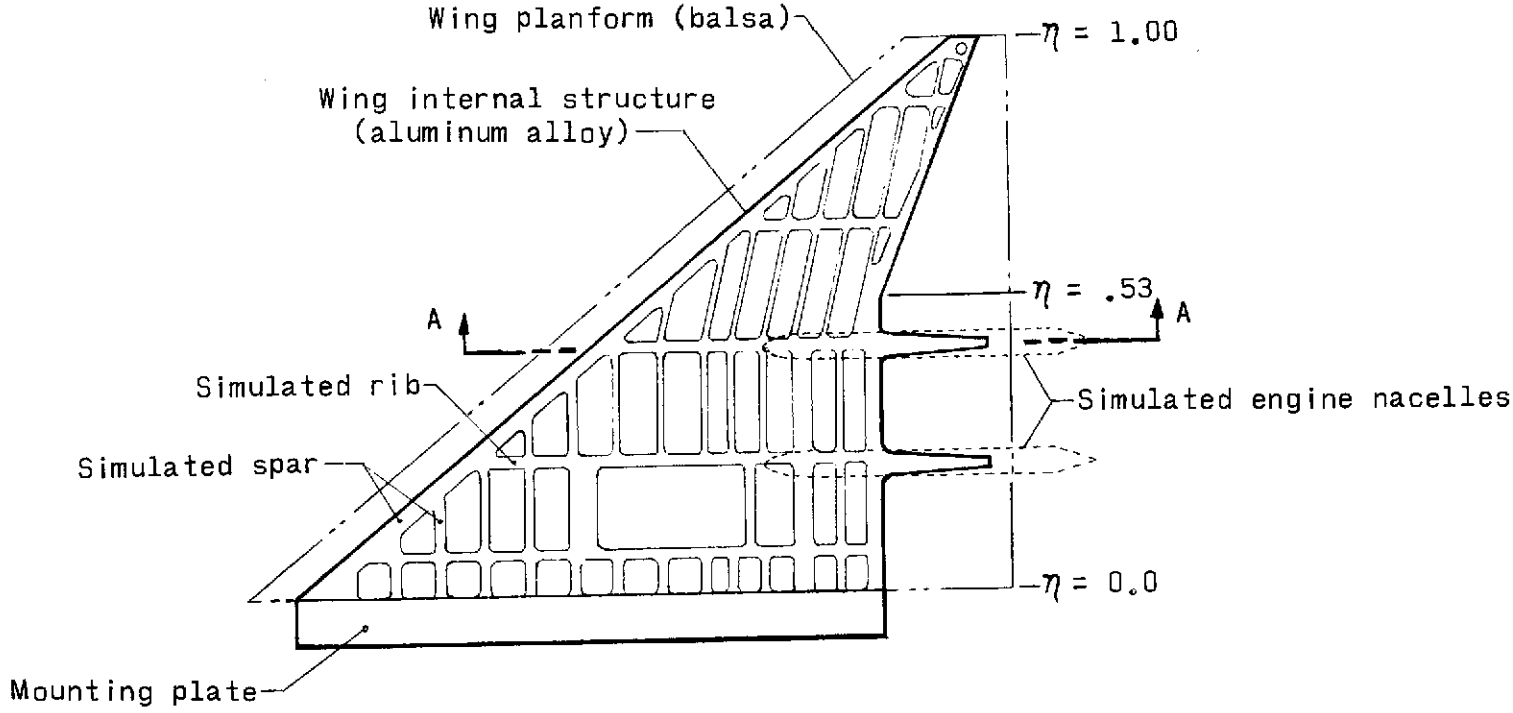

Figure 3.- Typical details of model construction.

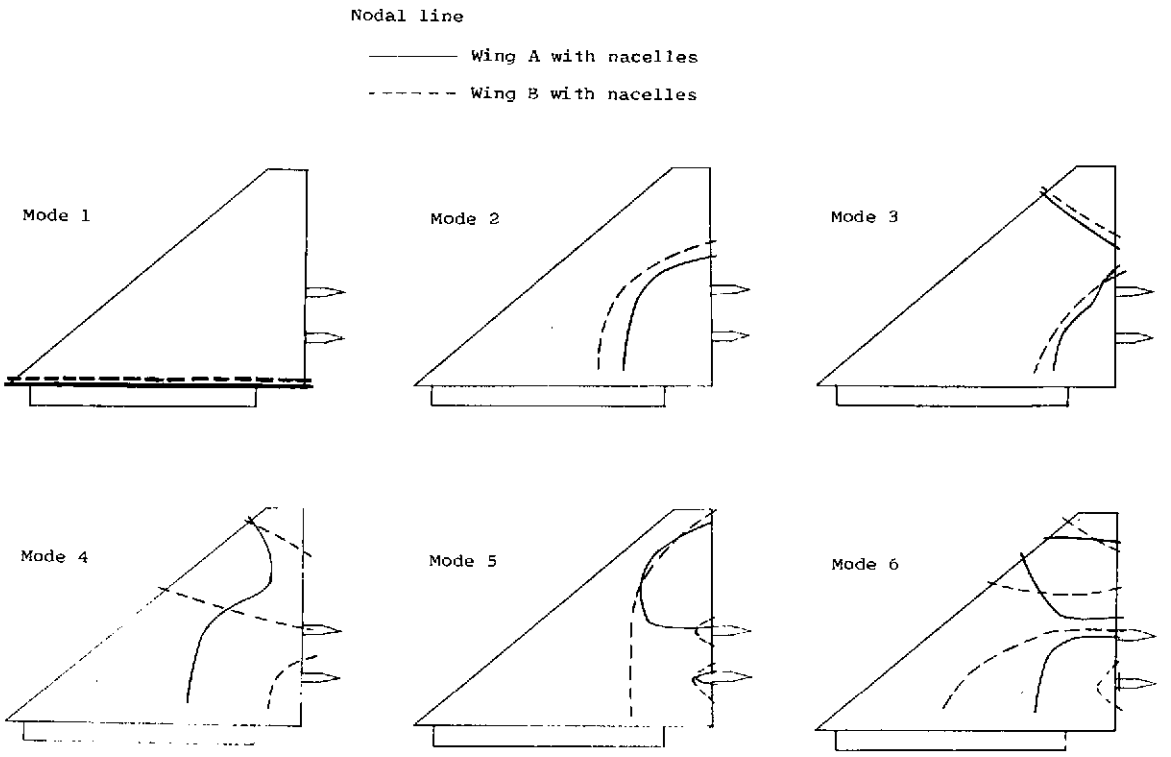

Vibration mode	Wing A		Wing B	
	Frequency, Hz	f_i/f_2	Frequency, Hz	f_i/f_2
1	18.65	0.54	13.69	0.46
2	34.65	1.00	29.55	1.00
3	58.30	1.68	50.40	1.71
4	102.20	2.95	83.50	2.83
5	114.00	3.29	106.20	3.59
6	136.00	3.93	119.60	4.05

Figure 4.- Measured nodal lines and frequencies of natural vibration modes for 1/36-size models in wind tunnel.

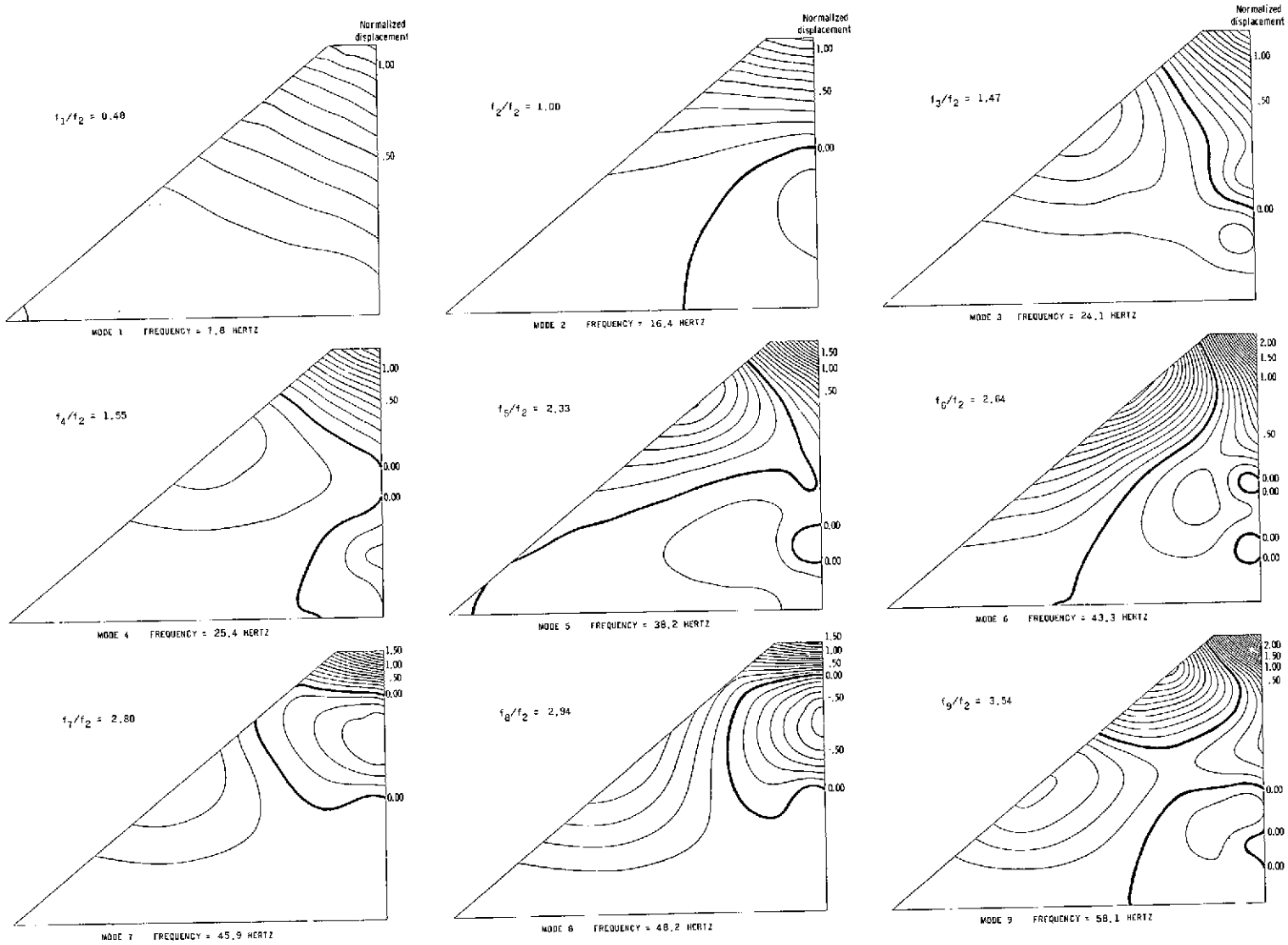

(a) Contour plots.

Figure 5.- Computer graphic display of measured mode shapes associated with natural vibration frequencies for 1/17-size model.

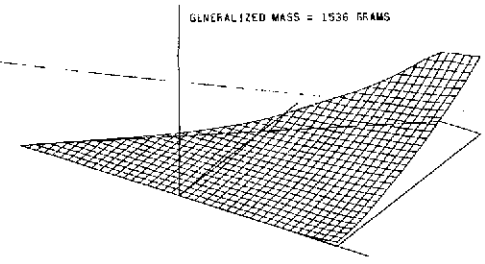

MODE 1 FREQUENCY = 7,8 HERTZ

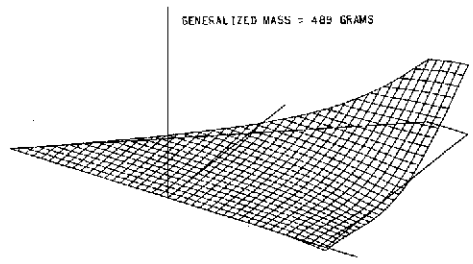

MODE 2 FREQUENCY = 16,4 HERTZ

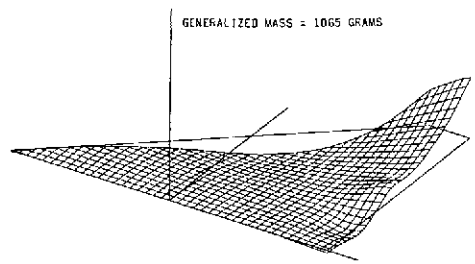

MODE 3 FREQUENCY = 24,1 HERTZ

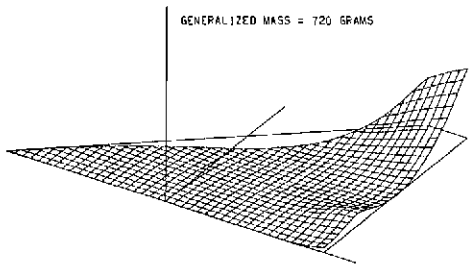

MODE 4 FREQUENCY = 25,4 HERTZ

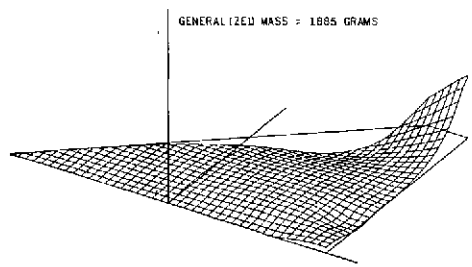

MODE 5 FREQUENCY = 38,2 HERTZ

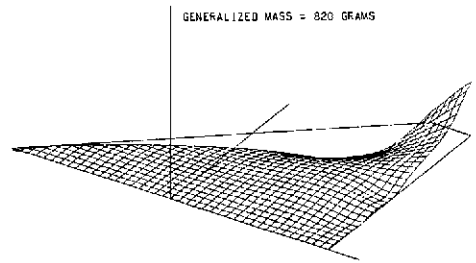

MODE 6 FREQUENCY = 43,3 HERTZ

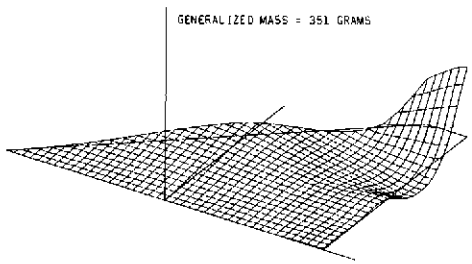

MODE 7 FREQUENCY = 45,9 HERTZ

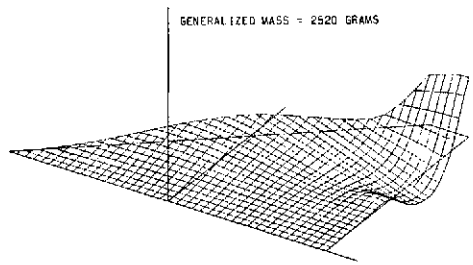

MODE 8 FREQUENCY = 48,2 HERTZ

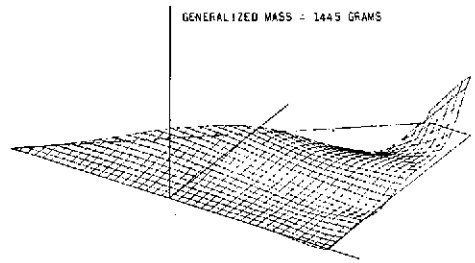

MODE 9 FREQUENCY = 58,1 HERTZ

(b) Oblique projection plots.

Figure 5.- Concluded.

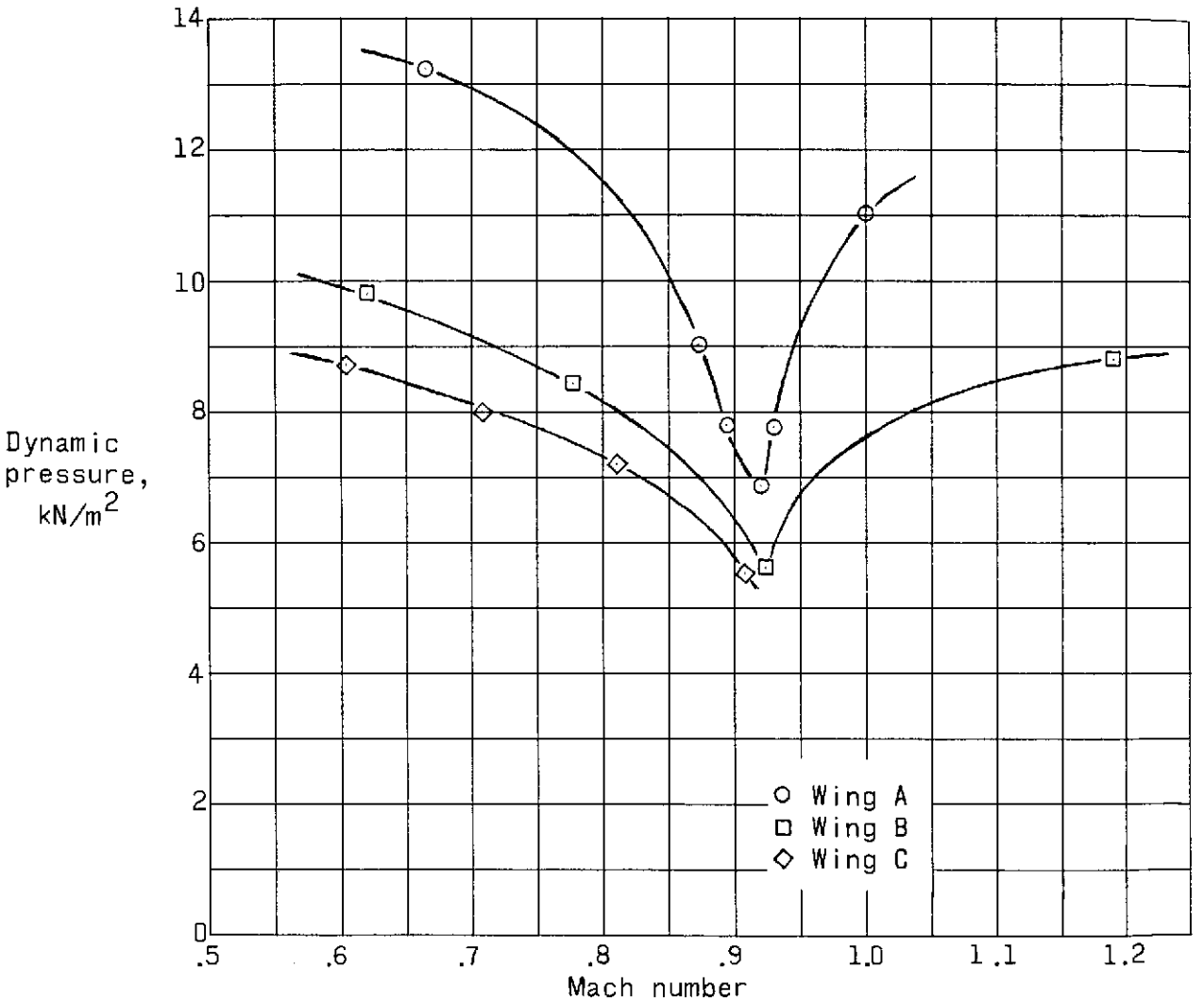

Figure 6.- Variation of flutter dynamic pressure with Mach number.

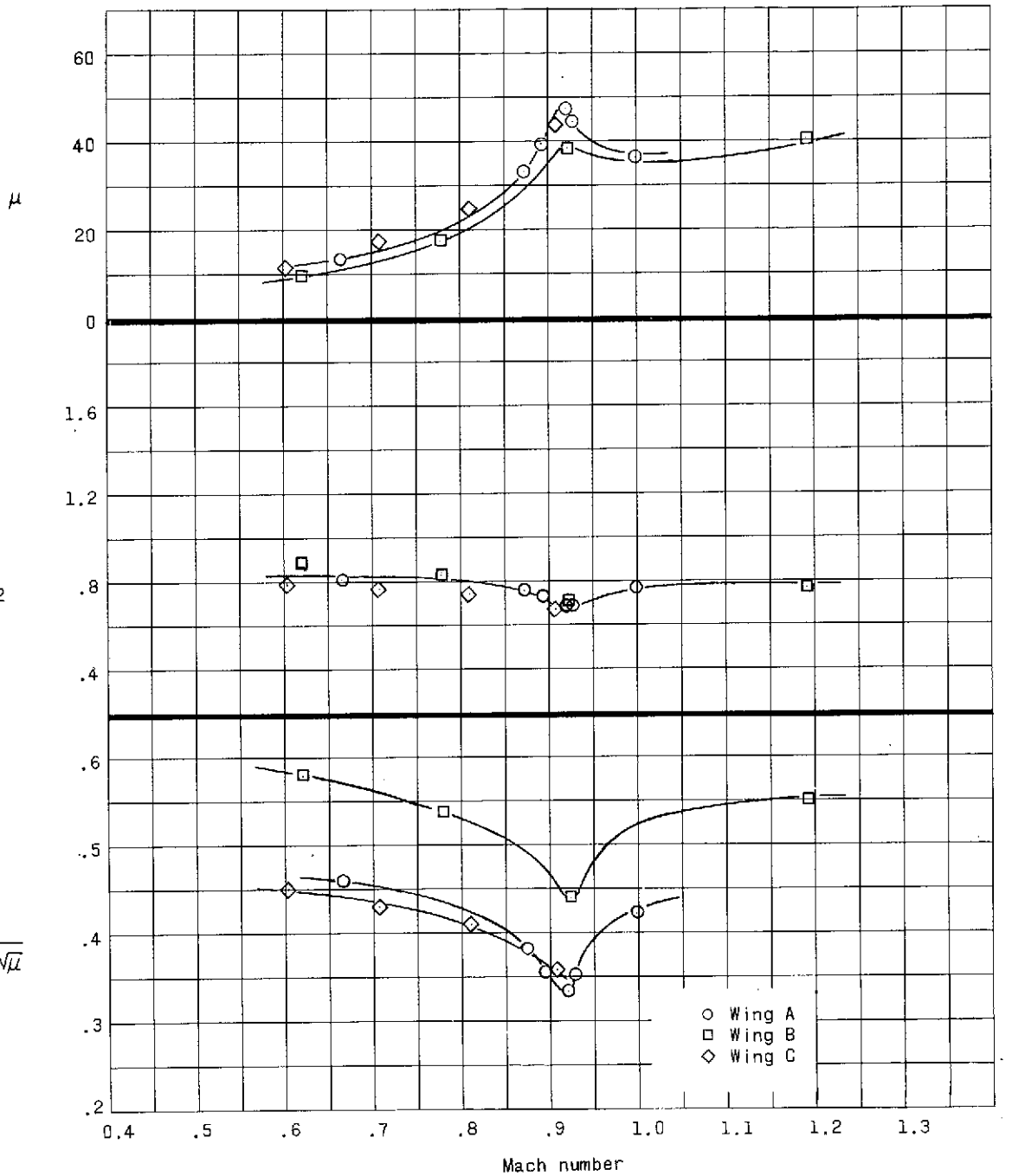

Figure 7.- Variation of flutter-speed index, flutter-frequency ratio, and mass-density ratio with Mach number.

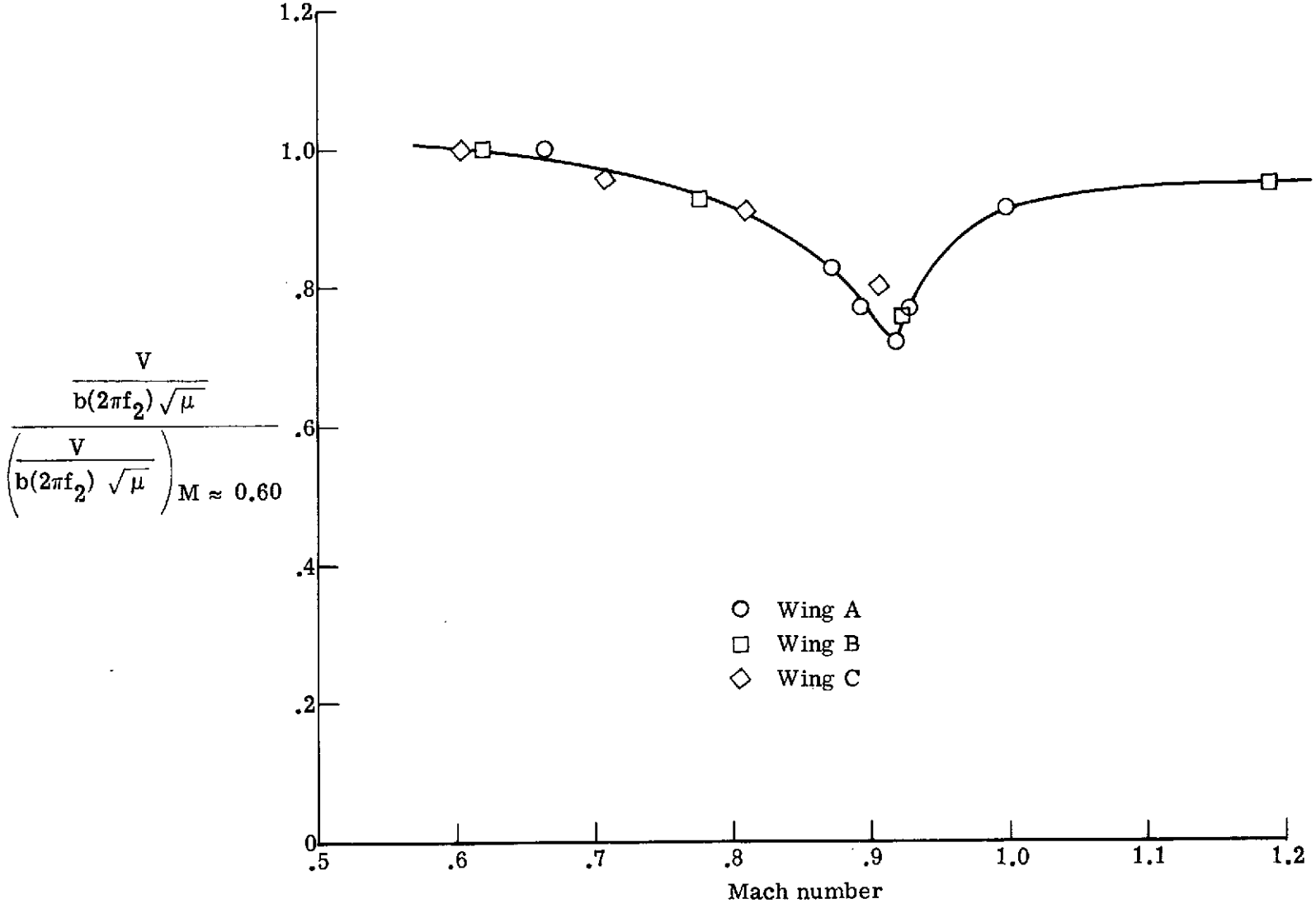

Figure 8.- Variation of normalized flutter-speed index with Mach number.

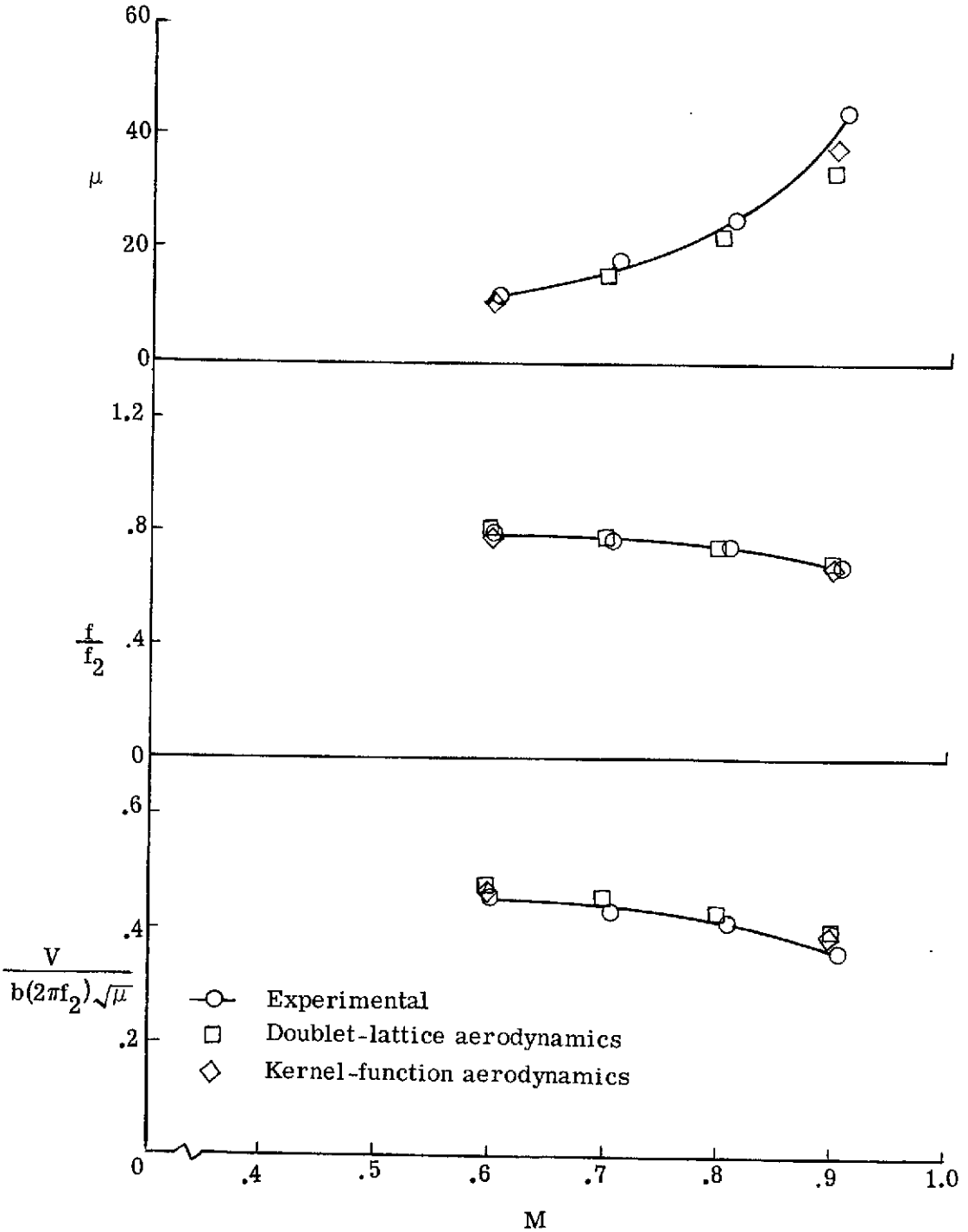

Figure 9.- Calculated and experimental flutter characteristics (wing C model).

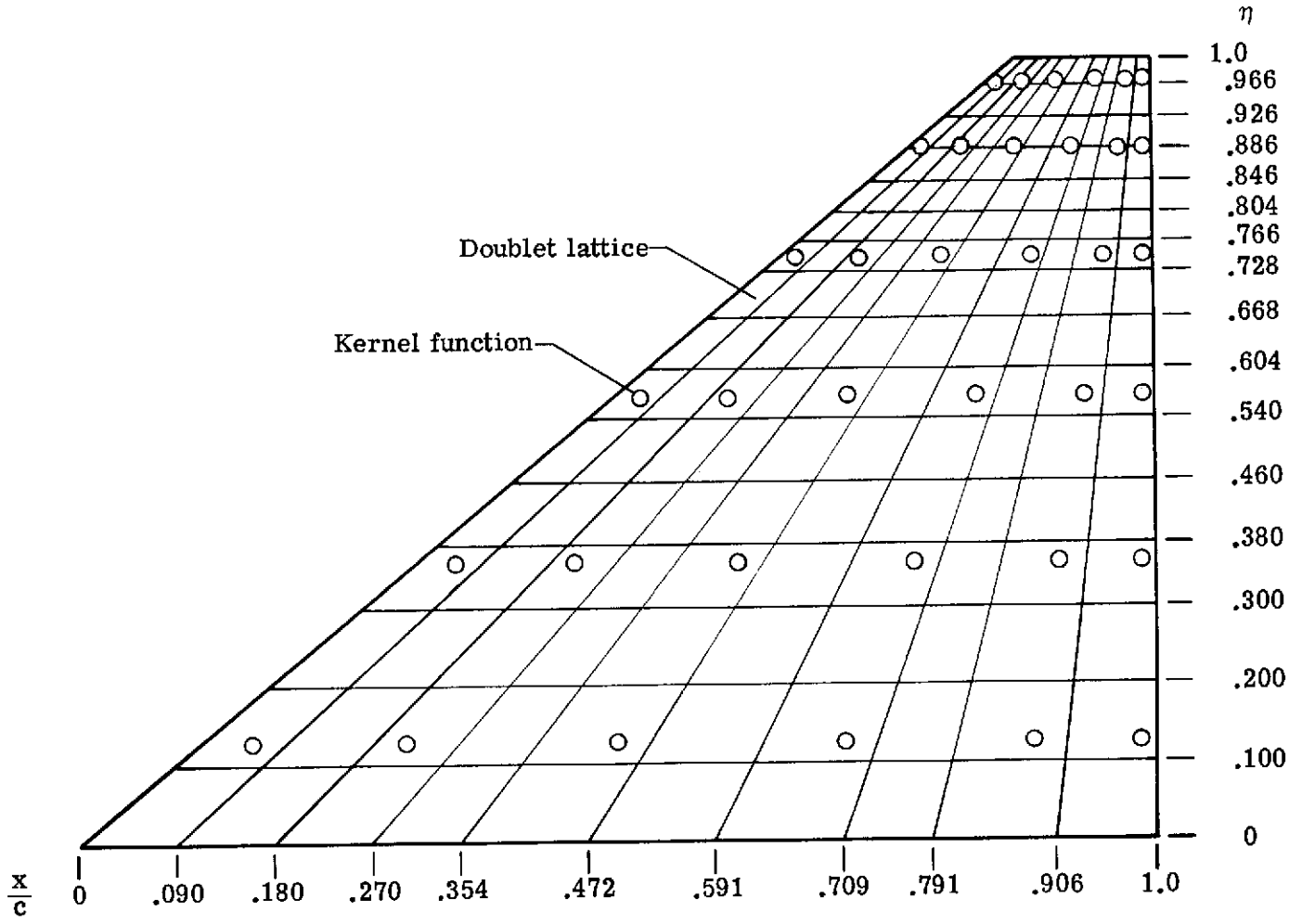

Figure 10.- Paneling scheme for doublet-lattice aerodynamics and collocation-point locations for kernel-function aerodynamics.

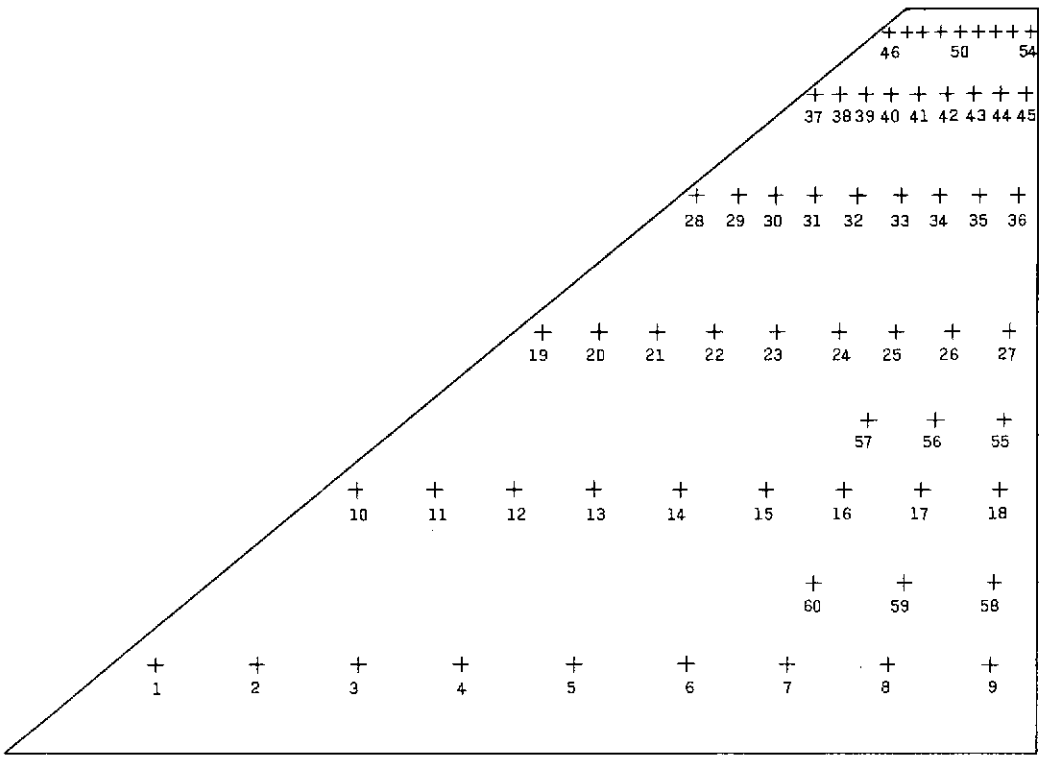

Pt	η	x/c	Pt	η	x/c	Pt	η	x/c	Pt	η	x/c	Pt	η	x/c	Pt	η	x/c
1	.1205	.05	10	.3546	.05	19	.5681	.05	28	.7485	.05	37	.8854	.05	46	.9709	.05
2	.1205	.16	11	.3546	.16	20	.5681	.16	29	.7485	.16	38	.8854	.16	47	.9709	.16
3	.1205	.27	12	.3546	.27	21	.5681	.27	30	.7485	.27	39	.8854	.27	48	.9709	.27
4	.1205	.38	13	.3546	.38	22	.5681	.38	31	.7485	.38	40	.8854	.38	49	.9709	.38
5	.1205	.50	14	.3546	.50	23	.5681	.50	32	.7485	.50	41	.8854	.50	50	.9709	.50
6	.1205	.62	15	.3546	.62	24	.5681	.62	33	.7485	.62	42	.8854	.62	51	.9709	.62
7	.1205	.73	16	.3546	.73	25	.5681	.73	34	.7485	.73	43	.8854	.73	52	.9709	.73
8	.1205	.84	17	.3546	.84	26	.5681	.84	35	.7485	.84	44	.8854	.84	53	.9709	.84
9	.1205	.95	18	.3546	.95	27	.5681	.95	36	.7485	.95	45	.8854	.95	54	.9709	.95

$Pt^{(1)}$	η	x/c	$Pt^{(1)}$	η	x/c
55	.4470	.95	58	.2290	.95
56	.4470	.84	59	.2290	.84
57	.4470	.73	60	.2290	.73

[1] Points 55 to 60 were added to define the nacelle motion for modes 3 to 9.

Figure 11.- Model control points (Pt) for vibration tests.